Food Chemistry 346 (2021) 128894

Contents lists available at ScienceDirect

Food Chemistry

journal homepage: www.elsevier.com/locate/foodchem

An insect acetylcholinesterase biosensor utilizing WO_3/g-C_3N_4 nanocomposite modified pencil graphite electrode for phosmet detection in stored grains

Sehrish Bilal [a,b], M. Mudassir Hassan [b], Muhammad Fayyaz ur Rehman [c], Muhammad Nasir [b], Amtul Jamil Sami [a,*], Akhtar Hayat [b,*]

[a] Institute of Biochemistry and Biotechnology, University of the Punjab, Lahore 54000, Pakistan
[b] Interdisciplinary Research Center in Biomedical Materials (IRCBM), COMSATS University, Islamabad, Lahore Campus, Lahore 54000, Pakistan
[c] Institute of Chemistry, University of Sargodha, Sargodha, Sargodha 40100, Pakistan

ARTICLE INFO

Keywords:
Acetylcholinesterase
Tribolium castaneum (Red flour beetle)
Pencil graphite electrode (PGE)
Graphitic carbon nitride
Tungsten oxide
Phosmet
Docking

Chemical compounds studied in this article:
Acetylthiocholine chloride (PubChem CID22411)
Potassium ferrocyanide ($K_4[Fe(CN)_6]$) (PubChem CID11963580)
Potassium ferricyanide ($K_3[Fe(CN)_6]$) (PubChem CID26250)
Phosmet (PubChem CID12901)
EDC (1-Ethyl-3-(3-dimethylaminopropyl) carbodiimide) (PubChem CID2723939)
MES (4-morpholinoethanesulfonic acid) (PubChem CID78165)
NHS (*N*-hydroxysuccinimide) (PubChem CID80170)
Melamine ($C_3H_6N_6$) (PubChem CID7955)

ABSTRACT

This study was undertaken to assess the potential of *Tribolium castaneum* (Red flour beetle) acetylcholinesterase (Tc-AChE) based electrochemical biosensor integrating WO_3/g-C_3N_4 nanocomposite modified Pencil graphite electrode to detect an organophosphate insecticide, Phosmet. The WO_3/g-C_3N_4 nanocomposite provides a non-toxic, biocompatible surface for binding the enzyme on the electrode surface, attributed to its large surface area, high conductivity, and low ohmic resistance. The proposed biosensor shows a very good analytical performance with LOD 3.6 nM for Phosmet and effectively determined Phosmet in wheat with a 99% recovery rate. Furthermore, molecular docking deciphers the binding interactions of Phosmet with Tc-AChE using a modified AutoDock LGA algorithm and an AMBER03 force field in YASARA. The kinetic parameters strongly suggest the high potency of inhibitor with the enzyme. This study presents an adaptable, rapid, and straightforward approach that opens ways towards real progress in developing commercial biosensors for pesticide detection.

1. Introduction

Pesticides are widely used agrochemicals that protect plants from pests or plagues and promote agricultural productivity. However, the extensive use of pesticides on crops and seeds is not a problem-free procedure for both consumers and the environment. The pesticides leave their degradation products called residues, in fields, water, or in air, which can enter human or animal bodies and cause severe nervous system problems, cancers, thyroid problems, and other potential health risks. Among these pesticides, Organophosphates (OP) are the third most commonly used pesticides in agriculture and household applications. OPs and their derivatives are the most toxic agricultural wastes having the potential to cause long term effects on human health due to their acute toxicity and bioaccumulation effects (Howard, Sage, Jarvis, & Gray, 1990). To ensure food safety among organisms, European Union (EU) has set certain standards, including a fixed Maximum residue limit

* Corresponding authors.
E-mail addresses: sehrishbilal@cuilahore.edu.pk (S. Bilal), mudassirhassan.27@cuilahore.edu.pk, muhammadnasir@cuilahore.edu.pk (M. Mudassir Hassan), amtuljamilsami@yahoo.com (A. Jamil Sami), akhtarhayat@cuilahore.edu.pk (A. Hayat).

https://doi.org/10.1016/j.foodchem.2020.128894
Received 23 June 2020; Received in revised form 5 November 2020; Accepted 13 December 2020
Available online 7 January 2021
0308-8146/

(MRL), which is the highest level of pesticide residues that can be legally tolerated in human and animal feeds. EU ensures that pesticides approved by EU regulation should not contain any harmful substances (Ionel, 2016a, 2016b, 2016c, 2016d). So far, United States Environmental Protection Agency (US-EPA) has forbidden the use of almost 270 pesticides to prevent the harmful effects of those pesticides on humans (Hamilton et al., 2004). Therefore, developing a rapid, sensitive, and practical method to detect trace amounts of these hazardous pesticide residues in agricultural products is of great importance.

Biosensors have recently taken over previous time-consuming and laborious pesticide determination methods due to their ease of performance, high sensitivity, robustness, and relatively low cost. Thus far, a great advancement in the construction of electrochemical biosensors for organophosphate pesticide determination has been made based on their ability to inhibit acetylcholinesterase (AChE), which is an important nervous system enzyme located at postsynaptic neuromuscular junctions and is involved in the termination of nerve impulses. Inhibition of AChE leads to ACh accumulation in the neuro-synapse resulting in prolonged neuro-excitation, causing muscular paralysis due to cholinergic poisoning. OPs are potent inhibitors of AChE and work by phosphorylating the main active site residue serine. The working principle of these biosensors depends on OPs high affinity towards AChE, which causes a decrease in AChE hydrolysis. Consequently, the extent of thiocholine production is reduced and the presence of pesticide is indirectly detected. The peak of the oxidation current of thiocholine upon applied potential is a measure of enzyme activity (Pumera, Sánchez, Ichinose, & Tang, 2007; Wang et al., 2020). Commonly used OPs include chlorpyrifos, dichlorvos, diazinon, malathion, parathion, methyl-parathion, fenitrothion, Phosmet, etc. Phosmet (2-(dimethoxyphosphinothioylsulfanylmethyl)isoindole-1,3-dione) is a very important and most commonly used organophosphate insecticide in Europe and its use was approved in 2007 for 14 years. The exposure of this pesticide to agricultural workers can lead to cholinergic poisoning, and it also poses ecological risks (Hernández-Borges, Cabrera, Rodríguez-Delgado, Hernández-Suárez, & Saúco, 2009). Phosmet residues that remain in treated products are considered a serious risk for consumer health.

For the construction of an AChE inhibition-based biosensor for Phosmet determination, two main approaches can be employed. The first concerns the selection of a suitable bio-recognition element and the second involves the modification of the transducer surface. Nowadays, nanocomposites are considered attractive candidates for making biosensor interfaces because of their remarkable catalytic and electrochemical properties, which can be utilized to upgrade the quality of electrochemical biosensors to meet basic commercial requirements (Awual et al., 2020; Awual, 2017, 2019a, 2019b, 2019c; Li, Singh, Li, & Banerjee, 2011; Pumera et al., 2007).

Nanocomposites based on graphene and its derivatives have enticed much attention in sensing applications; however, their 2D analogs such as graphitic carbon nitride (g-C_3N_4) possess exceptional catalytic, optical, thermal, and mechanical properties. Their preparation is very easy and economical compared to the lengthy procedures of graphene production (Thangavel, Elayaperumal, & Venugopal, 2012; Yang et al., 2013). The g-C_3N_4 (GCN), however, alone does not possess good electrical conductance, which can be improved by doping or coupling them with other nanomaterials such as tungsten trioxide (WO_3) (Chen et al., 2013; Kroke et al., 2002). Tungsten trioxide is a direct bandgap semiconductor having a bandgap of 2.5–2.8 eV with good electron transfer properties (ca. 12 $cm^2 V^{-1} s^{-1}$), which makes it an excellent choice for g-C_3N_4 nanocomposite preparation. WO_3/g-C_3N_4 nanocomposites have previously found applications in photocatalysis, but in this research, we explored its conductive properties to prepare a novel electrochemical biosensor for Phosmet determination in real agriculture samples (Thangavel et al., 2012; Wang et al., 2016). The great potential of WO_3/g-C_3N_4 nanocomposite is attributed to its large surface area, low ohmic resistance, and synergistic catalytic effect. Further, the lead pencil graphite electrode (PGE) ensures good adsorption of nanocomposite, is robust, and provides low background current.

As far as the biological element is concerned, most studies are based on commercial or genetically modified enzymes that are expensive and not easily available. However for limited-resource settings, scientists can opt for crude enzyme sources. The use of crude enzyme offers benefits like low cost of fabrication and high durability. Moreover, the crude extracts mimic enzyme's natural environment; therefore, provide enhanced bioavailability of cofactors and internal mediators, like stabilizers and activators, which are required for proper enzyme functioning. The AChE is a polymorphic enzyme and the catalytic subunit of the enzyme contains glycans in its native conformation, which are vital for acetylcholine synthesis. Not only, the purification of enzyme disturbs its native conformation, the available methods of purification are tedious, and expensive and final yields are relatively low. The problems related to sensitivity and selectivity can be improved by incorporating a highly efficient transducer surface using nanocomposite, which provides outstanding electrochemical behavior (Colmati, Sgobbi, Teixeira, Vilela, Martins, & Figueiredo, 2019). *Tribolium castaneum* (Red flour beetle) is a major pest of stored grains and is also a well-known model pest for scientific studies mainly because of its ease of culture and low maintenance requirements. *T. castaneum* produces high levels of AChE and the inhibition mechanisms of its various enzymes have also been studied in detail (Sami & Shakoori, 2014; Sami et al., 2016, 2018; Sami, 2014). The crude extracts of *T. castaneum* in the suitable buffer can provide an alternative to commercially available enzymes.

In this study, the catalytic and electrochemical properties of novel WO_3/g-C_3N_4 nanocomposite were anticipated to improve the electrochemical properties of the modified transducer surface towards the fabrication of *T. castaneum* acetylcholinesterase-based biosensor. Secondly, in addition to pesticide detection in food samples, the proposed method can be easily extended to study the inhibition of Acetylcholinesterase *in vivo* to understand the impact of pesticides on insects. Additionally, the proposed immobilization can serve as a generic platform to immobilized bio-receptors of all types, including enzyme, antibody, etc. to construct enzymatic/antibody-based biosensors for diverse applications.

2. Experimental

2.1. Materials

Acetylthiocholine chloride (ATCl) (>99% purity), Potassium ferrocyanide ($K_4[Fe(CN)_6]$), and Potassium ferricyanide ($K_3[Fe(CN)_6]$) were obtained from Sigma-Aldrich Corp. USA. Phosmet was purchased from Santa Cruz, Biotechnology, USA. EDC (1-Ethyl-3-(3-dimethylaminopropyl) carbodiimide) and MES (4-morpholinoethanesulfonic acid) were obtained from Tokyo chemical company (TCI), Japan, and NHS (*N*-hydroxysuccinimide) was obtained from CovaChem, USA. Melamine ($C_3H_6N_6$), Ascorbic acid, Citric acid, Glucose, and other chemicals, used for electrochemical analysis, were purchased from DAEJUNG, Chemicals & Metals Co., ltd. All chemicals were of analytical grade and used without further purification. Distilled water was acquired from ultrapure purification equipment. All solutions were freshly prepared for experiments and stored at 4 °C.

2.2. Instruments

The molecular bond information and functional groups of the composite were analyzed by Fourier Transform Infrared Spectroscopy (FTIR) at a scan range of 600–4000 cm^{-1} using Thermo Fischer Scientific (Nicolet 6700, USA) spectrometer (Gerwert & Kötting, 2001). Raman spectra were achieved using the In-Via Raman microscope (Renishaw, UK) with an excitation wavelength of 514 nm (Graves & Gardiner, 1989). The surface area and micropore size of the prepared samples were calculated by the BET and *t*-plot method by nitrogen adsorption at

77 K using TriStar II 3020 surface area analyzer. For this, the soak time was 0–999 min, ramp rate was 5–20 °C/min, ramp and soak cycles were up to 5 and the flow rate was 0–500 cm^3/min. All samples were degassed at 453 K for 4 h before starting adsorption–desorption measurements (Brunauer & Emmett, 1937).

Cyclic voltammetry and electrochemical impedance spectroscopy experiments were carried out on Interface 1010E^{TM} potentiostat (Gamry Instruments, USA). The cell consisted of a standard three-electrode system, including Ag/AgCl (1 M KCl) as a reference electrode, and the auxiliary electrode was a platinum wire. The working electrode was pencil graphite electrode (PGE), by Staedtler Mars GmbH & Co. KG, Germany, with pencil lead of 0.5 mm diameter and 60 mm length. A 5 mM solution of $K_4[Fe(CN)_6]/K_3[Fe(CN)_6]$(1:1) in 0.1 M KCl as an electrolyte was used for electrochemical experiments. For CV measurements, the potential for electrolyte was −0.8 V to + 0.8 V and the scan rate was 50 mVs^{-1}. Whereas the frequency of AC impedance was ranged from 0.1 MHz to 0.1 Hz, and amplitude was set at 233. For all other CV measurements, 0.1 M PBS (pH 8) was used.

2.3. Synthesis of bulk g-C_3N_4

Graphitic carbon nitride (g-C_3N_4) was synthesized in bulk by using a thermal polymerization method (Zhu et al., 2017). In this process, 5 g of melamine was added into a crucible and transferred to a muffle furnace at 450 °C in air atmosphere with a heating rate of 5 °C/min at ambient temperature and kept at this temperature for 3 h. The ramp rate was 10 °C/min at ambient pressure. After attaining the specific temperature and time, yellowish agglomerates were collected and ground in a mortar to form a fine powder for subsequent studies.

2.4. Synthesis of WO_3/g-C_3N_4 nanocomposite

For the synthesis of WO_3/g-C_3N_4 nanocomposite, 0.5 g of prepared g-C_3N_4 and 0.05 g of WO_3 (10:1) was suspended in 50 mL of distilled water. The prepared suspension was stirred for 30 min and then ultrasonicated for 1 h. The precipitates were collected by centrifugation at 1200 rpm for 10 min. The obtained precipitates were dried at 80 °C for 10 h in an oven and ground in a mortar to make a fine powder. The same procedure was followed to prepare the other two concentrations (i.e., 10:3, 10:4) just by varying quantities of WO_3. The prepared nanocomposites were further characterized for evaluating their surface area, chemical bonding, functional group analysis, and electrochemical response.

2.5. Insects culture and rearing

Cultures of Red flour beetle, *Tribolium castaneum* (Herbst) (Coleoptera: Tenebrionidae) have been obtained from local food stores and were reared and maintained on whole wheat flour at 37 °C and 65 ± 5% relative humidity (Sami et al., 2016).

2.6. Preparation of enzyme extract

40 mg of fifth instar larvae of *T. castaneum* (Red flour beetle) were homogenized in 50 μL of 0.1 M PBS (pH 8) and centrifuged at 10,000 rpm for 5 min. The resulting supernatant was used as an enzyme source for Acetylcholinesterase. 5 μL of the above extract was treated with 1.5 μL of 100 mM EDC/MES/NHS solution in order to activate the carboxyl groups for the coupling of primary amines to make amide bonds. NHS is used with EDC to produce stable amine-reactive intermediates, which helps in the immobilization of proteins by increasing the coupling efficiency. The MES acts as a coupling buffer for the activation reaction to occur. EDC/NHS coupling maximizes the chances of specific binding of the enzyme on the electrode surface by forming amide bonds (Fischer, 2010). The AChE/EDC/NHS/MES solution was sonicated for 5 min and was used for biosensor fabrication.

2.7. Fabrication of AChE/WO_3/GCN/PGE biosensor

The AChE/WO_3/GCN/PGE electrochemical biosensor was fabricated by the method demonstrated in Fig. 1. Firstly, 1 mg/mL WO_3/GCN nanocomposite suspension was prepared in distilled water by mixing and sonication. After electrochemical characterization of the material, WO_3/GCN (10:4) was selected for biosensor fabrication based on its high electrochemical response. WO_3/GCN (10:4) was further treated with a solution of 1 mM NaOH (w/v) and 0.5 mM Chloroacetic acid (w/v), to introduce carboxyl functional groups on the nanocomposite surface. The acid solution was mixed with nanocomposite suspension thoroughly by sonication for 20 min and then centrifuged for 10 min at 12000 rpm. The supernatant was discarded and the pellet was suspended in 1 mL of deionized water for further use. Before each experiment, the pencil graphite electrodes were cleaned electrochemically in 0.5 M H_2SO_4 and washed with distilled water. After the cleaning procedure, the electrodes were modified with WO_3/GCN (10:4) nanocomposite by immersing the tip of electrode in 2.5 μL of nanocomposite suspension for 15 min. The modified electrodes were removed and dried and then washed with distilled water to remove any unbound material and again air-dried before further modification. For enzyme immobilization, the nanocomposite coated electrodes were immersed in 5 μL of AChE/EDC/NHS/MES solution for 15 min, removed, and dried under laboratory conditions. The electrodes were again washed with distilled water to remove unbound enzyme or any impurity. The biosensor construction process was based on the making of amide bonds between the carboxyl group-containing material and EDC/NHS coupled biomolecule. The fabricated electrodes were stored at 4 °C when not in use.

2.8. Biosensor assay procedure

For amperometric measurement of the biosensor, cyclic voltammetry of AChE/WO_3/GCN/PGE, AChE/PGE and WO_3/GCN/PGE electrodes were carried out in 0.1 M PBS (pH 8) electrolyte solution, containing 8 mM ATCl, at potential ranging from 0 to 1 V and scan rate 50mVs^{-1}. For each measurement, a freshly prepared substrate solution was used. The same procedure was employed for the optimization of standard assay parameters.

Furthermore, Phosmet was selected as a model inhibitor to inspect the sensitivity of AChE/WO_3/GCN/PGE biosensor to detect organophosphate pesticides. The optimum incubation time of the inhibitor was determined by pre-incubating biosensor in 50 mM of pesticide solution for a time period of 5 to 60 min. For inhibition studies, the fabricated biosensor was dipped in different concentrations of pesticide solution for 30 min and the CV was taken. The percentage inhibition was calculated as a relative decrease in current after incubation with Phosmet and a calibration plot was formed using the following formula:

$$I\% = \frac{Ic - Ii}{Ic} x100$$

where I_c is the oxidation peak current for thiocholine, and I_i is the oxidation peak current for thiocholine in the presence of inhibitor (pesticide).

2.9. Extraction of pesticide from wheat samples

To assess the applicability of the biosensor, whole wheat flour was used as a real sample. The 2 g samples of wheat flour, with the mass-based on dry weight, were spiked with three different concentrations of Phosmet, i.e., 5 nM, 200 nM, and 800 nM, diluted in acetone. The acetone was evaporated under the fume hood at RT. The spiked wheat samples were mixed with 4 mL of acetonitrile: PBS (6:4, v: v) extraction solvent. The mixture was incubated for 10 min at room temperature and then centrifuged at 12,000 rpm for 5 min. The resulting supernatant was collected in separate Eppendorf tubes, which was employed as a

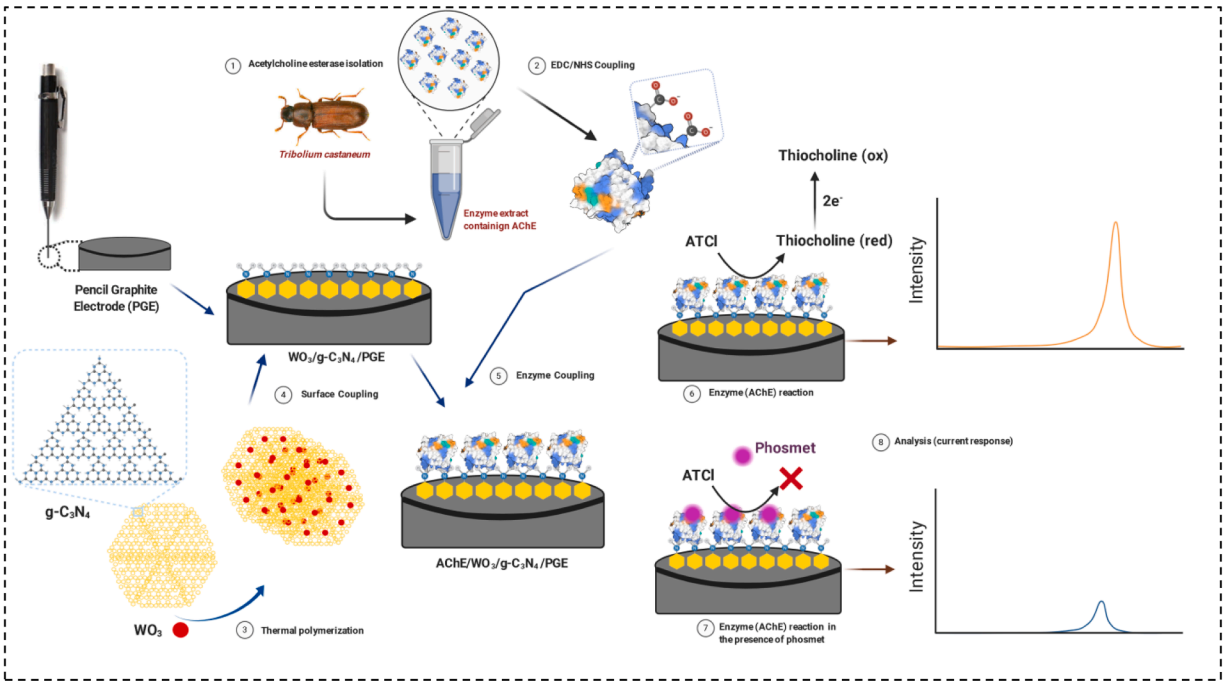

Fig. 1. Schematic illustration for the fabrication of AChE/WO_3/GCN/PGE biosensor for Phosmet detection, created by BioRender.

pesticide mother solution.

The phosmet content was estimated as percentage recoveries of added pesticide concentrations through biosensor method and the results were compared with standard HPLC method. HPLC analysis was carried out with a Thermo Scientific™ Hypersil™ BDS C18 reverse phase column (250 × 4.6 mm, 5 µm) using acetonitrile: PBS (65:35, v/v) mobile phase. The injection volume was 25 µL and flow rate was adjusted at 1 mL min^{-1}. The Phosmet was detected at 228 nm. Similarly, the wheat flour samples suspected to be contaminated with phosmet were obtained from local market and analyzed in the same manner for pesticide contamination.

2.10. Computational studies

2.10.1. Ligand and protein structure preparation

Three-dimensional ligand structures for Phosmet and Acetylthiocholine were obtained in structure data format (SDF) from PubChem (https://pubchem.ncbi.nlm.nih.gov) with CIDs: 12901 and 20544, respectively.

2.10.2. Molecular modelling

Tc-AChE is not available in RCSB Protein Data Bank (PDB) and was obtained by homology modeling performed using YASARA (Yet Another Scientific Artificial Reality Application) Structure version 20.1.18 (Krieger & Vriend, 2014). High-resolution, closely related X-ray Acetylcholinesterase structures with PDB IDs 6ARY (*Anopheles gambiae*), 5YDH (*Anopheles gambiae*), 5YDJ (*Anopheles gambiae*), 6G1U (*Torpedo californica*), 6QAA (*Homo sapiens*), were used to build the homology model. Side-chains were optimized and tuned, loop regions were built and a steepest descent, simulated annealing minimization was performed to refine the homology model. The best-obtained homology model was validated by the PROCHECK server (http://www.ebi.ac.uk/thornton-srv/software/PROCHECK/), VERIFY 3D (http://services.mbi. ucla.edu/Verify_3D/) and Ramachandran plot distribution.

2.10.3. Molecular docking simulations

To compare the efficacy of Phosmet *in silico* against Tc-AChE, ligand–protein binding energies were calculated using YASARA Structure software version 20.1.18 (Krieger & Vriend, 2014) with a modified AutoDock LGA algorithm and an AMBER03 force field. A number of 100 global docking runs were performed for one docking with a random seed value of 1000. The same force field was used for further energy-minimization for each ligand pose and rescored using AutoDock local search (LGA-LS), while keeping it confined to the original ligand pose. Active/binding site residues, binding energies, and dissociation constants were calculated for each ligand with the respective protein. Best docking poses with the lowest binding energy were extracted and ligand–protein interactions were visualized by PyMOL (The PyMOL Molecular Graphics System, Version 2.0 Schrödinger, LLC) and mapped using LigPlus (Laskowski & Swindells, 2011).

2.11. Repellency bioassay

To understand the impact of the organophosphate pesticide, Phosmet on *T. castaneum* larvae, an *in vivo* repellency bioassay was performed. For this purpose, a filter paper disc was cut with a diameter of about 1 in. and four equal quadrants were marked on petri plates. The filter paper disc was soaked in 1 mg/mL of Phosmet solution in acetone. The disc was placed in the first quadrant and acetone was air dried. Then, 10 larvae were released in that quadrant and the movement of insects was recorded from 0 to 7 min. The control experiment was arranged in the same manner using filter paper disc soaked in mere acetone (Sami et al., 2016).

3. Results and discussion

3.1. Characterization of WO_3/g-C_3N_4 nanocomposite

Fig. 2A is showing FTIR spectra of bulk g-C_3N_4 and WO_3/g-C_3N_4 composites having variable WO_3 content. For bulk g-C_3N_4, the peak at wavenumber 800 cm^{-1} is attributed to out of plane CN heterocyclic bending modes. Besides, the peak at 812 cm^{-1} indicates the breathing mode of triazine units, which is typical of the g-C_3N_4 structure. However, in the case of WO_3/g-C_3N_4 composites, the O-W-O absorption peak observed at 810 cm^{-1} seems overlapped, possibly due to a higher concentration of g-C_3N_4. Moreover, a set of peaks in the region from 1200

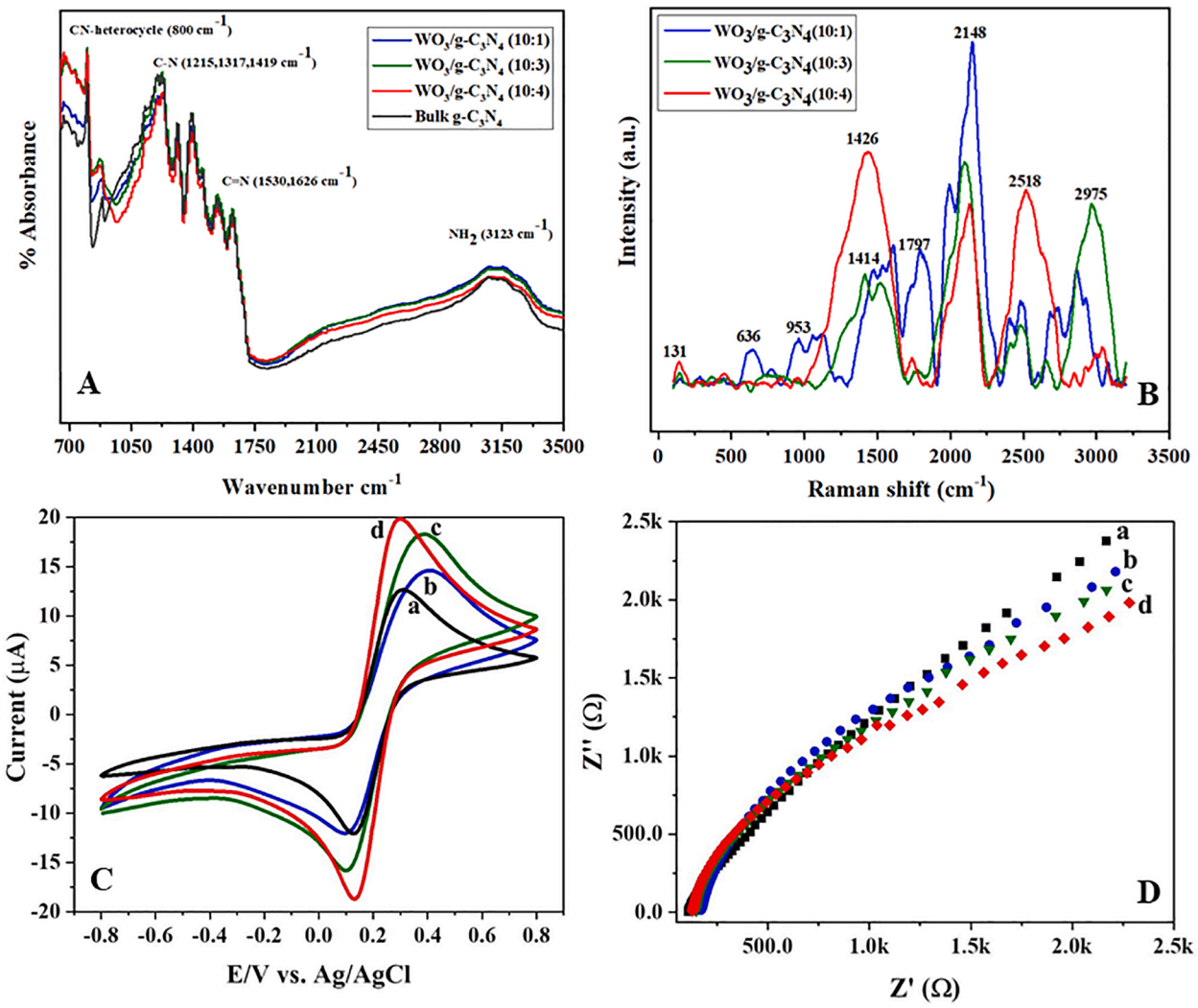

Fig. 2. (A) FTIR and (B) Raman spectra of Bulk g-C_3N_4 and WO_3/g-C_3N_4 nanocomposites with varying concentrations of WO_3. [Color codes: black (Bulk g-C_3N_4); blue (WO_3/g-C_3N_4, 10:1; green (WO_3/g-C_3N_4, 10:3), red (WO_3/g-C_3N_4, 10:4)]. (C) Cyclic voltammograms of WO_3/g-C_3N_4 nanocomposites deposited on the surface of PGE [a(black) : bare PGE, b(blue): WO_3/g-C_3N_4(10:1)/PGE, c(green): WO_3/g-C_3N_4 (10:3)/PGE, d(red): WO_3/g-C_3N_4 (10:4)/PGE)], using 5 mM $K_3[Fe(CN)_6]/K_4[Fe(CN)_6]$ in 0.1 M PBS at scan rate 50mVs^{-1}, and, (D) Electrochemical impedance Nyquist plots [a(black): bare PGE, b(blue): WO_3/g-C_3N_4(10:1)/PGE, c(green): WO_3/g-C_3N_4 (10:3)/PGE, d(red): WO_3/g-C_3N_4 (10:4)/PGE] at a frequency range of 0.1 MHz to 0.1 Hz. (For interpretation of the references to color in this figure legend, the reader is referred to the web version of this article.)

cm^{-1} –1400 cm^{-1} are associated to aromatic C—N stretching. The peaks at 1530 and 1626 cm^{-1} belong to cyano terminal groups C═N group of triple bond (Han et al., 2018). A broad peak at 3123 cm^{-1} can be seen in the right corner, which has been originated due to amine N—H stretching that occurs because some nitrogen groups partially get hydrogenated during the calcination process (Yang et al., 2013).

BET based on N_2 absorption was utilized to measure the pore size and specific surface area of the prepared composite. The BET specific surface area of three WO_3/g-C_3N_4 composites having ratios 10:1, 10:3 and 10:4 are 6.96, 8.62, and 8.84 m^2/g, respectively. Similarly, the average pore size diameter of the composites was measured as 19.88, 19.85, and 20.04 Å, respectively (Table S1). The obtained data showed that with the increase in the amount of WO_3, both the surface area and pore size of the composites increased. The increase in surface area signifies an improvement in the electron transfer properties and reactivity of the composite (Fig. S1). Although the surface area was not increased to a larger extent, an improvement in the surface area was observed to enhance the catalytic efficiency. The aim of the employed material was not only to increase the surface area but also to increase the electrons and hole pairs production and reduce the recombination of these produced electrons and holes by the introduction of WO_3 in g-C_3N_4. The results also confirmed the increased electrochemical response of the electrodes by increasing the concentration of WO_3, which is a good advancement.

Raman spectroscopy was conducted to further investigate the molecular structure and interaction between WO_3 and g-C_3N_4 after the formation of the nanocomposite. Fig. 2B shows the Raman spectra of WO_3/g-C_3N_4 nanocomposite with its different compositions. A small peak can be seen at 131 cm^{-1}, attributed to the O-W-O bending mode, while a peak at 636 cm^{-1} indicates the stretching vibration of O-W-O. Further, a peak at 953 cm^{-1} arose due to the symmetric stretching mode of the terminal W = O bond. A higher peak was observed at 1426 cm^{-1}, attributed to C—N bending vibration, whereas the peaks at 2148 cm^{-1} and 2518 cm^{-1} indicate C═N bending modes. The last peak at 2975 cm^{-1} is associated with amine N—H stretching vibrations. The results confirmed that the number of constituent atoms of WO_3 is higher in WO_3/g-C_3N_4 (10:4). It is also noteworthy that peaks for WO_3 are sharper, suggesting the crystalline nature of WO_3, whereas peaks for g-C_3N_4 are broader, indicating the amorphous phase of g- C_3N_4.

3.2. Electrochemical characterization of electrodes

The three WO_3/g-C_3N_4 composites were compared for their electrochemical performance. For this purpose, CV and EIS of modified electrodes were performed. Cyclic voltammetry (CV) was done to determine the conductivity of modified electrodes using a 5 mM equimolar solution of $K_3[Fe(CN)_6]/K_4[Fe(CN)_6]$ in 0.1 M KCl. As shown in Fig. 2C, the redox current is considerably increased in the case of WO_3/g-C_3N_4 (10:4). Further, electrochemical impedance spectroscopy (EIS) was performed to examine the interfacial properties and transfer of electrons on the modified electrode's surface. The diameter of the semicircle in the Nyquist plots is related to the electron transfer resistance (Rct) at high frequencies, and the linear trend is shown at low frequencies. As shown in Fig. 2D, resistance to electron transfer is noticeably decreased in the case of WO_3/g-C_3N_4 (10:4). The results indicate that the charge transfer resistance is decreased ascribing to the high electrical conductivity of the nanocomposite modified electrode. The electroactive surface area of bare and WO_3/g-C_3N_4 modified PGE was determined from the peak current obtained by cyclic voltammograms by using the Randles-Sevsic equation, which came out to be 0.148 cm^2 and 0.23 $cm^{2,}$ respectively (Bard, Faulkner, Leddy, & Zoski, 1980). The increased active surface area of the nanocomposite modified electrode implies to the increase in adsorption of electrochemical probes and enhanced catalytic performance of biosensor. So, WO_3/g-C_3N_4 (10:4) was chosen further for the fabrication of the biosensor.

Later the selected nanocomposite was treated with NaOH and chloroacetic acid to introduce carboxyl functional groups on the surface in order to improve the chances of specific binding of the enzyme by forming C—N bonds (Chen et al., 2013). As shown in Fig. S2A, the introduction of COO^- increases the electron transfer resistance, thereby reducing redox peak current and increasing impedance. The results confirmed the presence of COO^- functional groups on the nanocomposite surface. Furthermore, the immobilization of insect AChE on the nanocomposite modified electrode further increased the hindrance to electron transfer owing to the insulator nature of biomolecules, thus ensures successful attachment of enzyme molecules on the electrode surface (Fig. S2B). Therefore, surface architecture and catalytic properties of WO_3/g-C_3N_4 nanocomposite were utilized to create an interface ensuring the specific binding of AChE on the surface of the pencil graphite electrode.

3.3. Analytical performance of biosensor

The electrochemical behavior of the fabricated biosensor was

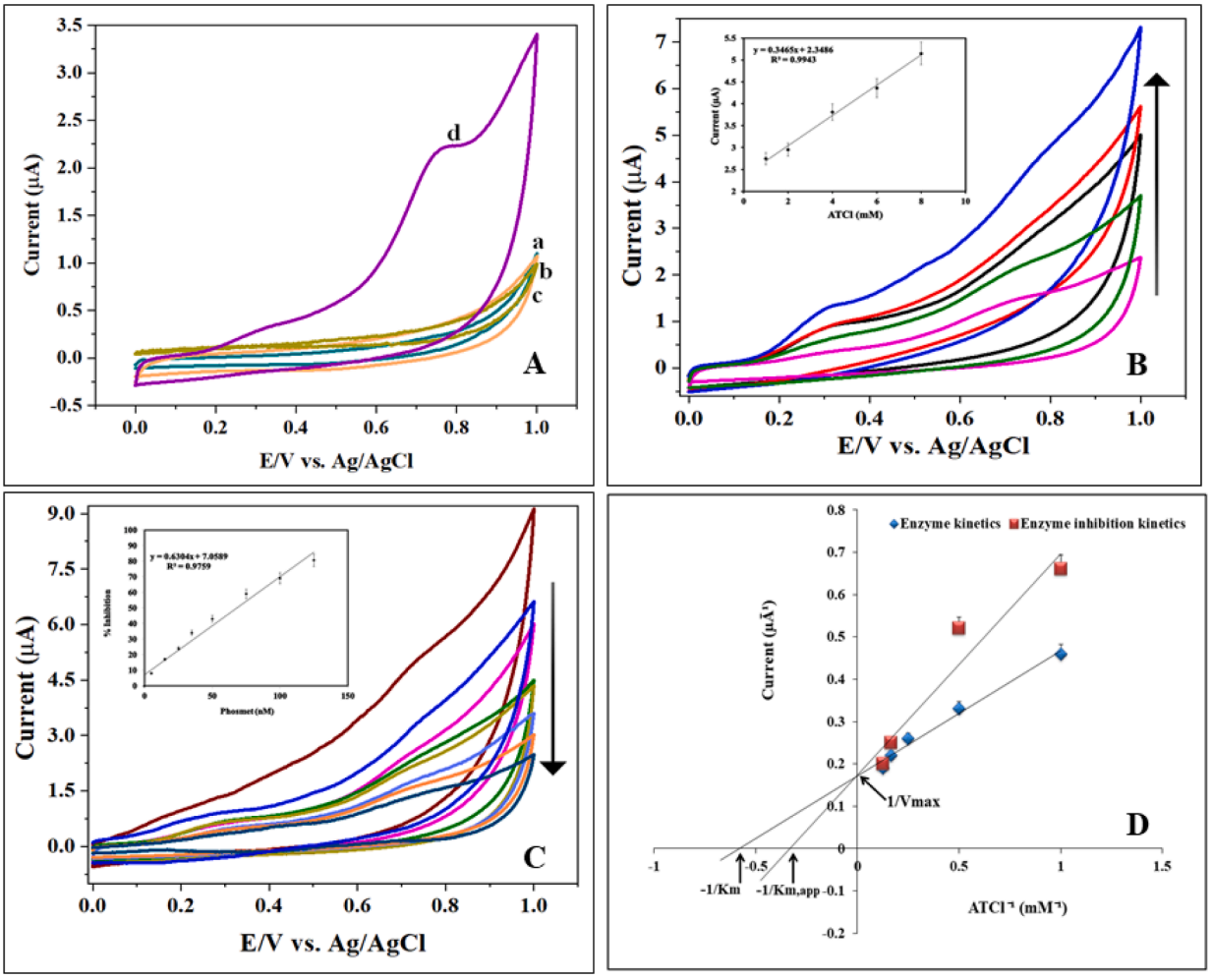

Fig. 3. Cyclic voltammograms of bare PGE(a-turquoise), AChE/PGE(b-green), WO_3/GCN/PGE(c-yellow) and AChE/WO_3/GCN/PGE(d-purple) modified with 5 µL of 15 mg/ml enzyme-containing extract in 0.1 M PBS (pH-8) containing 8 mM ATCl at 50mVs^{-1} by sweeping the potential between 0 and 1 V (A), Current response of AChE/WO_3/GCN/PGE biosensor with increasing concentrations of ATCl: inset shows the calibration curve of current against the concentration of ATCl (B), CV curves of biosensor after incubating with different concentrations of Phosmet in 0.1 M PBS (pH-8) containing 8 mM ATCl: inset shows calibration plot for Phosmet detection at a linear range of 0 to 125 nM (C), Lineweaver-Burk plots (1/S vs1/Ipa) of ATCl without (blue line) and with inhibitor (red line) indicating same Vmax and different Km depicting competitive inhibition of Tc-AChE with Phosmet (imidan). (For interpretation of the references to color in this figure legend, the reader is referred to the web version of this article.)

determined by cyclic voltammetry. Fig. 3A shows the current response of WO_3/GCN/PGE, AChE/PGE, and AChE/WO_3/GCN/PGE in 0.1 M PBS (pH 8) containing 8 mM ATCl. The figure reveals that no detectable peak generated in the case of bare PGE, AChE/PGE, and WO_3/GCN/PGE. However, in AChE/WO_3/GCN/PGE biosensor, an obvious irreversible oxidation peak was detected at 0.74 V as a result of hydrolysis of ATCl into thiocholine, which is an electroactive moiety. The peak current signal was measured as a difference between the baseline and plateau current intensity. The results explained that AChE activity predominantly increased when incorporated with nanocomposite. It has been proved that the increase in the oxidation peak current of thiocholine is attributed to the synergistic catalytic effect of the interface of WO_3/GCN. The large active surface area attained by the deposition of nanocomposite on the electrode surface not only causes an increase in the oxidation of thiocholine but also provides an excellent platform for enzyme immobilization on the electrode surface without disturbing its original conformation and catalytic activity. It can be inferred that the proposed bio-surface improves enzyme stability and analytical performance of biosensor.

To determine whether the electrode reaction is adsorption or diffusion-controlled, the electrochemical response was measured by varying scan rate in 0.1 M PBS containing ATCl (Fig. S3). Results show a good linear response between the current and square root of scan rate, the linear regression equation is Ipa (μA) = $0.0603v^{1/2}$ (mVs^{-1}) + 1.7373, R^2 = 0.9386, indicating the process is most likely diffusion controlled. The linear regression equation for plot of log Ipa and logv is Log Ipa (μA) = 0.1004logv (mVs^{-1}) + 0.1691, R^2 = 0.9728. Therefore, the anodic behavior can be identified as a diffusion-controlled process.

3.4. Optimization of experimental parameters

To maximize the amperometric response of the devised biosensor, various parameters such as incubation time of material and enzyme, amount of enzyme, scan rate and pH were optimized. First, the optimum incubation time for material deposition was studied to obtain a high amperometric response, and it turned out that 15 min are enough to obtain maximum current response (Fig. S4A). Next, the pH of the buffer was optimized to evaluate the sensitivity of the biosensor, as pH plays a very significant role in enzyme activity. Slight changes in pH affect the bioactivity of AChE as changes in ionization of the active site of enzyme or substrate affect enzyme-substrate interactions. It may also affect the stability of material on the electrode surface. Ellman, 1961 and various others reported optimum pH for AChE activity to be 8, so electrochemical measurements with phosphate buffer of pH ranging from 6 to 8 were performed and pH 8 was selected, as the maximum current was obtained at this pH (Fig. S4B) (Ellman, Courtney, Andres, & Featherstone, 1961; Guler, Turkoglu, & Basi, 2017). Similarly, the incubation time of enzyme and the amount of enzyme is important to achieve a stable and broad linear response range (Fig. S4C and D). The biosensor was tested by increasing extract concentration, and the current response was increased at 40 mg extract concentration with 15 min of incubation. The specific activity of Tc-AChE at this concentration was 83.3 μA/cm^2. As we know that too low enzyme leads to a small current response as a result of insufficient product formation. On the other hand, high amounts of the enzyme may result in inefficient binding of the enzyme to the transducer surface, causing leakage of the enzyme from the surface. Moreover, higher enzyme amounts may increase the thickness of the electrode surface, thus elevating electrode resistance. Therefore, the amount is considered sufficient for electrode modification. Moreover, to get the best current response, scan rate was chosen to be 50 mVs^{-1} (Zhang et al., 2019).

The amperometric response of the biosensor in the presence of different substrate concentrations was also investigated. The biosensor displayed an increase in peak oxidation current with an increase in the concentration of ATCl in PBS (pH 8), and after a certain limit, a steady-state in the current was observed depicting substrate saturation. As shown in Fig. 3B, the biosensor exhibited a linear correlation between peak oxidation current and amount of substrate, ranging from 1 to 8 mM, given with an equation, I = 0.3465C + 2.3486 (R^2 = 0.9943). The LOD and sensitivity were found to be 0.9 mM and 8.25 μA$mM^{-1}cm^{-2}$, respectively. Moreover, the apparent Michaelis-Menten constant (Km) was calculated from the Lineweaver-Burk plot of 1/current vs 1/ATCl (Fig. S4E), which came out to be 0.59 mM. The value is lower than Km of AChE in solution-based assays as well as many other reported biosensors (Table S1). As is known that lower Km denotes a high affinity of the enzyme with substrate. The results revealed that the Tc-AChE is in a favorable orientation in the AChE/WO_3/GCN/PGE biosensor and is not desorbed during the biosensor fabrication. It can be inferred that the proposed sensing platform, by providing a biocompatible environment for the immobilization of AChE, reduces the leaching of the enzyme from the electrode surface, therefore increasing the stability of the biosensor.

3.5. Application of biosensor for Phosmet detection

To evaluate the usefulness of the proposed biosensor for the detection of organophosphate pesticides in agricultural products, Phosmet (Imidan) was selected as a model pesticide. The biosensor was pre-incubated with different concentrations of Phosmet for 30 min (Fig. S4F), and a decrease in current was observed with an increase in the concentration of Phosmet. The calibration curve was drawn under optimal conditions, using concentrations of Phosmet ranging from 5 nM to 800 nM. A linear response was found in the range from 5 nM to 125 nM with a correlation coefficient R^2 = 0.9759 (n = 8), showing good analytical performance of the biosensor (Fig. 3C). All the readings were taken in triplicates with RSD < 4% (n = 3). The limit of detection (LOD) and limit of quantification (LOQ) was calculated based on the standard deviation of the response and the slope of the calibration line, which came out to be 3.6 nM and 11.2 nM, respectively, and detection sensitivity was 15 μA$nM^{-1}cm^{-2}$. A high detection sensitivity and low detection limit ascertain that the sensing design exhibits properties useful for organophosphates determination in grains.

If we compare the detection limits with previously reported methods of Phosmet detection, Attaollah Shakoori, 2017, reported Phosmet detection in wheat by gas chromatography coupled with mass spectrometric detection in the selected ion monitoring mode (GC-SIM-MS) with LOD of 6.2 ng/g at a linear range 20–200 ng/g (Shakoori, Mahasti, & Moradi, 2017). Song, 2013 reported a surface plasmon resonance immunoassay for Phosmet detection in agriculture products with LOD 1.6 ng/L, but no study has been reported on wheat (Song, Liu, & Wang, 2013). The present work provides a novel biosensing design for understanding the importance of different methods for establishing the presence of these pesticide residues in other categories of plant-based foods and to practically facilitate the determination of Phosmet in stored grains such as wheat, under conditions of some low concentrations of this pesticide in the biomass.

3.6. Real sample analysis

The developed biosensor was tested to detect insecticide extracted from the spiked whole wheat flour samples. Samples confirmed as not containing the pesticide, were considered as blank and spiked wheat samples were used for recovery determination. As shown in Table 1, the percentage recoveries were found up to 99%, and obtained results were in agreement with the results of HPLC analysis. To evaluate the trueness of devised method a couple of locally obtained wheat samples were also tested with both biosensor and HPLC methods and obtained results were found comparable (Table 1).

The precision of the method in real sample analysis was validated by investigating the current response of different electrodes prepared in the same manner for determination of 50 nM Phosmet in wheat. The variability between electrodes was <10%. The results indicate that the developed biosensor could be used as a promising platform for Phosmet

Table 1
An analysis of percentage recovery of Phosmet in real samples.

Determination of Phosmet in spiked wheat flour samples								
	Phosmet Biosensor				HPLC			
Pesticide	Added concentration (nM)	Found concentration (nM)	Recovery %	RSD% (n = 3)	Added concentration (nM)	Found concentration (nM)	Recovery %	RSD% (n = 3)
Phosmet	5	4.6 ± 1	92	2.5	5	4.57 ± 2	91	2.1
	200	194 ± 2	97	1.7	200	196.8 ± 4	98	1.1
	800	794 ± 2	99	0.7	800	794.6 ± 2	99	1.5

Analysis of local wheat flour samples suspected to be contaminated with Phosmet.				
	Phosmet Biosensor		HPLC	
Samples	Concentration of Phosmet (nM)	RSD% (n = 3)	Concentration of Phosmet (nM)	RSD% (n = 3)
1	61 ± 4	3.5	62.8 ± 4	2.8
2	Uncontaminated	–	Uncontaminated	–
3	24 ± 4	3.5	28 ± 4	3.5

detection in wheat and other stored grains samples following a simple extraction protocol.

3.7. Method validation

The operational reproducibility of the biosensor was verified by taking CV measurements of 10 freshly prepared AChE/WO_3/GCN/PGE electrodes using 8 mM ATCl in PBS pH 8, and a mean current response of 4.5 ± 5 μA was obtained each time, showing good reproducibility of the biosensor with RSD < 6% (n = 10). The proposed method is robust and the fabricated biosensor gives response in just 1 min. Similarly, to evaluate the precision of the proposed sensor in the determination of Phosmet, the repeatability of results was investigated by taking four independent CV measurements using the same concentration of Phosmet and the RSD was < 7% (n = 4), which is satisfactory. Moreover, storage stability was determined by observing changes in the current response of AChE/WO_3/GCN/PGE biosensor by using extracts stored at 4 °C for up to 30 days. After 30 days period, the amperometric response was reduced to 60% of the original response.

In order to investigate the selectivity of the established biosensor, the effects of interfering species such as glucose, ascorbic acid, citric acid, heavy metals and inorganic ions were investigated on the detection of Phosmet by the biosensor (Fig. S5). No significant interfering effect was observed and results were in accordance with calculated values. However, ascorbic acid and citric acid strongly interfered with the response.

3.8. Enzyme inhibition kinetics

The deduced biosensor was found quite effective in describing the enzyme kinetics by electrochemical methods and the mechanism of inhibition is also well explained. The peak oxidation currents were recorded with increasing the amount of substrate in the absence and presence of inhibitor. The Lineweaver-Burk plots between 1/S and 1/Ipa revealed no change in Vmax of enzyme, while Km was increased in the presence of inhibitor, which proves the mechanism of inhibition of Tc-AChE by Phosmet is competitive. The affinity of inhibitor with Tc-AChE was determined by calculating the inhibition constant, Ki, for phosmet which came out to be 30 nM, which indicates the high potency of inhibitor with enzyme depicting high sensitivity of Tc-AChE enzyme with Phosmet (Fig. 3D). The results reveal that the proposed biosensor platform can be effectively used to study enzyme-inhibitor interactions as well as efficacy of an inhibitor against enzymes activity.

3.9. Computational analysis

The structural topographies required for the interaction of Tc-AChE with the substrate, Acetylcholine and inhibitor, Phosmet, were explored by molecular docking. Homology modelling templates contained at least 80% coverage (Table S3) and more than 60% sequence identity to obtain a good model. Model validation by the YASARA program shows quality Z-scores as 0.173, 0.211, and −1.646 for dihedrals, 1D and 3D packing, respectively, while the overall Z-score for the model was found to be −0.573 that shows a good model (Table S4). The overall Z-scores was calculated by weighing the averages of the individual Z-scores using the formula

$$\text{Overall Z - score} = 0.145^{*}Dihedrals + 0.390^{*}Packing1D + 0.465^{*}Packing3D$$

The Ramachandran plot shows 96% of residues in favored regions and 99.6% in allowed regions. Only two outliers were found, GLY^{209} and SER^{524}, on the basis of phi, psi angles and corrected with different rotamer selection.

Molecular docking shows that Phosmet interacts with Tc-AChE with a binding energy of −6.74 cal/mol and dissociation constant of 11.5 μM. The active site residues interacting with Phosmet include ILE^{138}, ILE^{139}, ASP^{140}, THR^{141}, VAL^{142}, TRP^{152}, ASN^{153}, GLY^{186}, TYR^{189}, SER^{190}, GLY^{191}, LEU^{195}, TRP^{348}, TYR^{396}, and TYR^{400} (Fig. 4A). Tyr^{189} and Ser^{190} are involved in making the H-bonds (3.11 and 3.40 Å) with O1 and N of Phosmet, respectively, while other surrounding residues are involved in stabilizing the interactions (Fig. 4B). In another binding pose, H-bonds with the bond length of 3.10 and 3.19 Å were found to interact with the same atoms in Phosmet (Fig. S7), while stabilizing active site residues were GLN^{137}, ILE^{138}, ILE^{139}, ASP^{140}, TRP^{152}, ASN^{153}, PRO^{154}, GLY^{186}, GLY^{187}, TYR^{189}, SER^{190}, GLY^{191}, LEU^{195}, GLU^{266}, SER^{267}, TYR^{396}, PHE^{397}, HIS^{507}, ALA^{508}, and ILE^{511}. The complex seems to be stable by π-π interactions of Phosmet and TYR^{189} rings (Awual, Yaita, Kobayashi, Shiwaku, & Suzuki, 2020). ILE^{139} shows hydrophobic contacts with Phosmet ring, whereas ALA^{508} has hydrophobic contacts with distal methyl groups in Phosmet (Fig. S7). Acetylthiocholine (ATC) has shown relatively weaker binding compared to Phosmet with a binding energy of −4.3 kcal/mol and with a dissociation constant of 498 μM (Fig. 4C). The active site residues involved were TRP^{152}, PHE^{184}, GLY^{185}, GLY^{186}, GLY^{187}, SER^{190}, GLY^{191}, THR^{192}, LEU^{195}, TYR^{198}, GLU^{266}, SER^{267}, TYR^{396}, PHE^{397}, HIS^{507}, ALA^{508}, and ILE^{511}. Three H-bonds were observed in ATC interactions with Tc-AChE, where GLY^{185} and GLY^{186} interact with O1 and O2 of ATC (Fig. 4D).

The analysis of docking solutions suggests that Phosmet can attach to the substrate-binding site of Tc-AChE through covalent and hydrophobic interactions and act as a potent inhibitor of Tc-AChE, as confirmed by our experimental findings. The results demonstrated that inhibitor binds with the catalytic site of the enzyme hence competitively inhibits Tc-AChE. The results are in agreement with experimental findings and provide additional support to our results. However, in physiological conditions where solvent and temperature conditions are maintained, the enzyme seems to work better. Future studies may involve MD simulations to work this out by *in silico* analyses.

3.10. Feeding behavior of insects to Phosmet

Many insects have reduced sensitivity against pesticides and produce

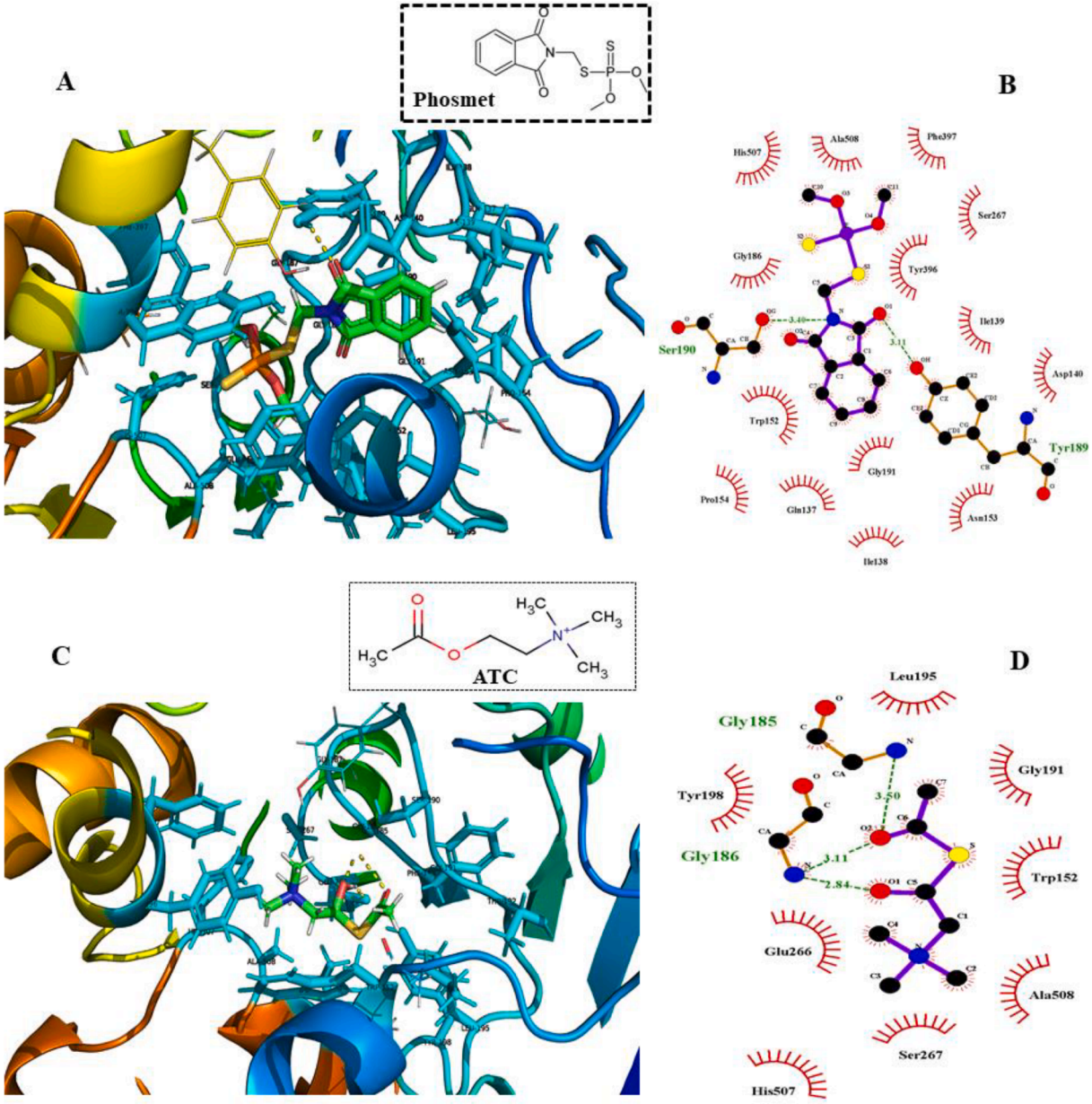

Fig. 4. Molecular docking analysis summary. Close-up view of docking complex of Tc-AChE and Phosmet: inset shows structure of Phosmet (A), Close-up view of docking complex of Tc-AChE and ATC: inset shows structure of ATC (C), LigPlot of binding interaction of amino acid residues of AChE with Phosmet (B) and ATC (D), where the arc with spokes radiating towards the ligand indicates hydrophobic contacts with ligand atoms and the spokes radiating back represent contacted atoms of ligand.

resistance against biological as well as chemical pesticides. There are many species of insects that have been declared resistant to various known pesticides. To determine the behavior of *T. castaneum* insects in response to Phosmet, an antifeedant bioassay was performed. The results showed that under a time period of 7 min, 50% of the *T.castaneum* larvae left the first quadrant and entered the second quadrant away from the area where the pesticide was present (Fig. 5). However, no repellent behavior has been observed in the control petri plate till a period of 7 min. The movement of larvae was recorded for every 30 s using a stopwatch and a graph has been formed between no. of insects that had left the inhibitor-containing first quadrant and entered the second quadrant (Fig. 5C), which shows that with time the number on insects retained in the first quadrant has reduced to half of the total insects present in that quadrant. The results gave an insight into the efficacy of Phosmet towards the insect's larvae. The toxicity can be evaluated in future work through controlled bioassays using different concentrations of pesticide.

4. Conclusion

This work deployed physicochemical properties of WO_3/g-C_3N_4 nanocomposite and potential of an insect AChE to construct a biosensor to detect Phosmet, which can kill pests of stored grains such as *Tribolium castaneum*. The study found that the nanocomposite had properties in order to construct a biosensing interface with good analytical performance. The transducer modification by WO_3/g-C_3N_4 nanocomposite improves the electron transfer between the enzyme and electrode surface, which in turn improves electrical conductivity and quality of output signal with minimal interfering effects. The developed biosensor was able to detect Phosmet in spiked wheat samples with good recovery rates. The work presented here has a dual importance in terms of establishing a method for sensitive detection of Phosmet in other

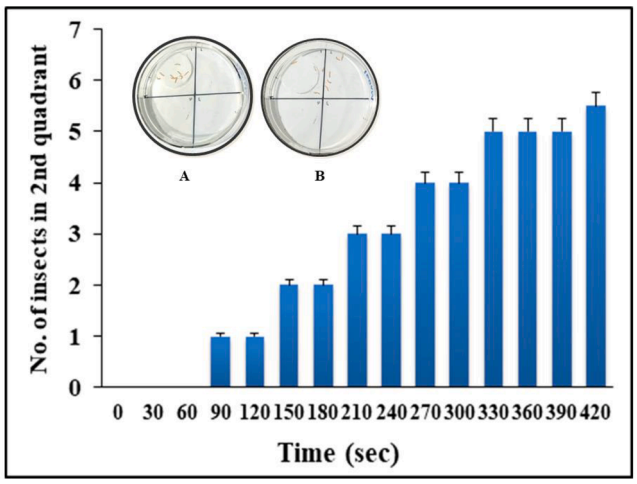

Fig. 5. Graph representing antifeedant behavior of *T.castaneum* larvae by an *in vivo* repellency bioassay. The number of insects decreased with time in the first quadrant containing inhibitor and increased in the second quadrant away from the inhibitor (inset shows movement of larvae in petri plates (A) without Phosmet and (B) with Phosmet).

categories of plant-based foods, as well as theoretically determining the binding interactions between enzyme and inhibitor through inhibition kinetics and molecular docking studies to understand the effectiveness of established methods and determining the impact of these chemical hazards on insects.

CRediT authorship contribution statement

Sehrish Bilal: Data curation, Writing - original draft, Software, Writing - review & editing. **M. Mudassir Hassan:** Data curation, Software. **Muhammad Fayyaz ur Rehman:** Writing - review & editing. **Muhammad Nasir:** Methodology, Resources, Investigation. **Amtul Jamil Sami:** Supervision, Methodology, Investigation, Validation. **Akhtar Hayat:** Supervision, Methodology, Resources, Investigation, Validation.

Declaration of Competing Interest

The authors declare that they have no known competing financial interests or personal relationships that could have appeared to influence the work reported in this paper.

Acknowledgements

This work was supported by COMSATS University through a research grant provided by Pakistan Science Foundation under project PSF-MSRTII/AGR/P-COMSATS-LHR (09)/2019.

Appendix A. Supplementary data

Supplementary data to this article can be found online at https://doi.org/10.1016/j.foodchem.2020.128894.

References

Awual, M. R. (2017). Novel nanocomposite materials for efficient and selective mercury ions capturing from wastewater. *Chemical Engineering Journal, 307*, 456–465. https://doi.org/10.1016/j.cej.2016.08.108.

Awual, M. R. (2019a). Innovative composite material for efficient and highly selective Pb (II) ion capturing from wastewater. *Journal of Molecular Liquids, 284*, 502–510. https://doi.org/10.1016/j.molliq.2019.03.157.

Awual, M. R. (2019b). Novel conjugated hybrid material for efficient lead(II) capturing from contaminated wastewater. *Materials Science and Engineering: C, 101*, 686–695. https://doi.org/10.1016/j.msec.2019.04.015.

Awual, M. R. (2019c). Novel ligand functionalized composite material for efficient copper(II) capturing from wastewater sample. *Composites Part B: Engineering, 172*, 387–396. https://doi.org/10.1016/j.compositesb.2019.05.103.

Awual, M. R., Hasan, M. M., Iqbal, J., Islam, A., Islam, M. A., Asiri, A. M., & Rahman, M. M. (2020). Naked-eye lead(II) capturing from contaminated water using innovative large-pore facial composite materials. *Microchemical Journal, 154*, 104585. https://doi.org/10.1016/j.microc.2019.104585.

Awual, M. R., Yaita, T., Kobayashi, T., Shiwaku, H., & Suzuki, S. (2020). Improving cesium removal to clean-up the contaminated water using modified conjugate material. *Journal of Environmental Chemical Engineering, 8*(2), 103684. https://doi.org/10.1016/j.jece:2020.103684.

Bard, A. J., Faulkner, L. R., Leddy, J., & Zoski, C. G. (1980). *Electrochemical methods: fundamentals and applications* (Vol. 2). wiley New York.

Brunauer, S., & Emmett, P. H. (1937). The use of low temperature van der waals adsorption isotherms in determining the surface areas of various adsorbents. *Journal of the American Chemical Society, 59*(12), 2682–2689. https://doi.org/10.1021/ja01291a060.

Chen, L., Huang, D., Ren, S., Dong, T., Chi, Y., & Chen, G. (2013). Preparation of graphite-like carbon nitride nanoflake film with strong fluorescent and electrochemiluminescent activity. *Nanoscale, 5*(1), 225–230. https://doi.org/10.1039/C2NR32248J.

Colmati, F., Sgobbi, L. F., Teixeira, G. F., Vilela, R. S., Martins, T. D., & Figueiredo, G. O. (2019). Electrochemical biosensors containing pure enzymes or crude extracts as enzyme sources for pesticides and phenolic compounds with pharmacological property detection and quantification. In Biosensors for Environmental Monitoring): IntechOpen.

Ellman, G. L., Courtney, K. D., Andres, V., jr., & Featherstone, R. M. (1961). A new and rapid colorimetric determination of acetylcholinesterase activity. *Biochemical Pharmacology, 7*(2), 88–95. https://doi.org/10.1016/0006-2952(61)90145-9.

Fischer, M. J. (2010). Amine coupling through EDC/NHS: A practical approach. In *Surface plasmon resonance* (pp. 55–73). Springer.

Gerwert, K., & Kötting, C. (2001). *Fourier transform infrared (FTIR) spectroscopy*. Wiley online library.

Graves, P., & Gardiner, D. (1989). *Practical raman spectroscopy*. Springer.

Guler, M., Turkoglu, V., & Basi, Z. (2017). Determination of malation, methidathion, and chlorpyrifos ethyl pesticides using acetylcholinesterase biosensor based on Nafion/Ag@rGO-NH2 nanocomposites. *Electrochimica Acta, 240*, 129–135. https://doi.org/10.1016/j.electacta.2017.04.069.

Hamilton, D., Ambrus, Á., Dieterle, R., Felsot, A., Harris, C., Petersen, B., Racke, K., Wong, S.-S., Gonzalez, R., Tanaka, K., Earl, M., Roberts, G., & Bhula, R. (2004). Pesticide residues in food-acute dietary exposure: Pesticide residues in food-acute dietary exposure. *Pest Management Science: formerly Pesticide Science, 60*(4), 311–339. https://doi.org/10.1002/ps.865.

Han, X., Xu, D., An, L., Hou, C., Li, Y., Zhang, Q., & Wang, H. (2018). WO_3/g-C_3N_4 two-dimensional composites for visible-light driven photocatalytic hydrogen production. *International Journal of Hydrogen Energy, 43*(10), 4845–4855. https://doi.org/10.1016/j.ijhydene.2018.01.117.

Hernández-Borges, J., Cabrera, J. C., Rodríguez-Delgado, M.Á., Hernández-Suárez, E. M., & Saúco, V. G. (2009). Analysis of pesticide residues in bananas harvested in the Canary Islands (Spain). *Food Chemistry, 113*(1), 313–319. https://doi.org/10.1016/j.foodchem.2008.07.042.

Howard, P. H., Sage, G., Jarvis, W., & Gray, D. (1990). Handbook of environmental fate and exposure data for organic chemicals. Volume II: solvents.

Ionel, B. (2016a). European Regulation in the Veterinary Sanitary and Food Safety Area, a Component of the European Policies on the Safety of Food Products and the Protection of Consumer Interests: A 2007 Retrospective. Part Four: Decisions. Universul Juridic, 24-27.

Ionel, B. (2016b). European Regulation in the Veterinary Sanitary and Food Safety Area, A Component of the European Policies on the Safety of Food Products and the Protection of Consumer Interests: A 2007 Retrospective. Part One: The Role of European Institutions in Laying Down and Passing Laws Specific to the Veterinary Sanitary and Food Safety Area. Revista Universul Juridic ISSN 2393-3445, 12-15.

Ionel, B. (2016c). European Regulation in the Veterinary Sanitary and Food Safety Area, a Component of the European Policies on the Safety of Food Products and the Protection of Consumer Interests: A 2007 Retrospective. Part Three: Directives. Universul Juridic, 20-23.

Ionel, B. (2016d). European Regulation in the Veterinary Sanitary and Food Safety Area, A Component of the European Policies on the Safety of Food Products and the Protection of Consumer Interests: A 2007 Retrospective. Part Two: Regulations. Revista Universul Juridic ISSN 2393-3445, 16-19.

Krieger, E., & Vriend, G. (2014). YASARA View—molecular graphics for all devices—from smartphones to workstations. *Bioinformatics, 30*(20), 2981–2982.

Kroke, E., Schwarz, M., Horath-Bordon, E., Kroll, P., Noll, B., & Norman, A. D. (2002). Tri-s-triazine derivatives. Part I. From trichloro-tri-s-triazine to graphitic C_3N_4 structures. *New Journal of Chemistry, 26*(5), 508–512.

Laskowski, R. A., & Swindells, M. B. (2011). LigPlot+: multiple ligand–protein interaction diagrams for drug discovery. In): ACS Publications.

Li, S., Singh, J., Li, H., & Banerjee, I. A. (2011). *Biosensor nanomaterials*. John Wiley & Sons.

Pumera, M., Sánchez, S., Ichinose, I., & Tang, J. (2007). Electrochemical nanobiosensors. *Sensors and Actuators B: Chemical, 123*(2), 1195–1205. https://doi.org/10.1016/j.snb.2006.11.016.

Sami, A. J. (2014). Azadirachta indica derived compounds as inhibitors of digestive alpha-amylase in insect pests: Potential bio-pesticides in insect pest management. *European Journal of Experimental Biology, 4*(1), 259–264.

Sami, A. J., Bilal, S., Khalid, M., Nazir, M. T., & Shakoori, A. (2018). A Comparative study of inhibitory properties of saponins (derived from Azadirachta indica) for Acetylcholinesterase of Tribolium castaneum and Apis mellifera. *Pakistan Journal of Zoology, 50*(2), 725–733.

Sami, A. J., Bilal, S., Khalid, M., Shakoori, F. R., Rehman, F., & Shakoori, A. (2016). Effect of crude neem (Azadirachta indica) powder and azadirachtin on the growth and acetylcholinesterase activity of Tribolium castaneum (Herbst)(Coleoptera: Tenebrionidae). *Pakistan Journal Zoology, 48*(3), 881–886.

Sami, A. J., & Shakoori, A. (2014). Potential of Azadirachtin and neem (Azadirachta indica) based saponins as biopesticides for in vitro insect pests cellulase (Beta-1, 4-Endoglucanase) enzyme inhibition and in vivo repellency on Tribolium castaneum. *Biotechnology Journal International*, 904–917.

Shakoori, A., Mahasti, P., & Moradi, V. (2017). Determination of twenty organophosphorus pesticides in wheat samples from different regions of Iran. Iranian Journal of Toxicology, 11(5), 37-44.

Song, Y., Liu, M., & Wang, S. (2013). Surface plasmon resonance sensor for phosmet of agricultural products at the ppt detection level. *Journal of Agricultural and Food Chemistry, 61*(11), 2625–2630. https://doi.org/10.1021/jf304997r.

Thangavel, S., Elayaperumal, M., & Venugopal, G. (2012). Synthesis and properties of tungsten oxide and reduced graphene oxide nanocomposites. *mat express, 2*(4), 327–334. https://doi.org/10.1166/mex.2012.1087.

Wang, T., Quan, W., Jiang, D., Chen, L., Li, D.i., Meng, S., & Chen, M. (2016). Synthesis of redox-mediator-free direct Z-scheme AgI/WO_3 nanocomposite photocatalysts for the degradation of tetracycline with enhanced photocatalytic activity. *Chemical Engineering Journal, 300*, 280–290. https://doi.org/10.1016/j.cej.2016.04.128.

Wang, W., Wang, X., Cheng, N., Luo, Y., Lin, Y., Xu, W., & Du, D. (2020). Recent advances in nanomaterials-based electrochemical (bio)sensors for pesticides detection. *TrAC Trends in Analytical Chemistry, 132*, 116041. https://doi.org/10.1016/j.trac.2020.116041.

Yang, S., Gong, Y., Zhang, J., Zhan, L., Ma, L., Fang, Z., Vajtai, R., Wang, X., & Ajayan, P. M. (2013). Exfoliated graphitic carbon nitride nanosheets as efficient catalysts for hydrogen evolution under visible light. *Adv. Mater., 25*(17), 2452–2456. https://doi.org/10.1002/adma.201204453.

Zhang, P., Sun, T., Rong, S., Zeng, D., Yu, H., Zhang, Z.e., Chang, D., & Pan, H. (2019). A sensitive amperometric AChE-biosensor for organophosphate pesticides detection based on conjugated polymer and Ag-rGO-NH2 nanocomposite. *Bioelectrochemistry, 127*, 163–170. https://doi.org/10.1016/j.bioelechem.2019.02.003.

Zhu, M., Zhai, C., Sun, M., Hu, Y., Yan, B.o., & Du, Y. (2017). Ultrathin graphitic C_3N_4 nanosheet as a promising visible-light-activated support for boosting photoelectrocatalytic methanol oxidation. *Applied Catalysis B: Environmental, 203*, 108–115. https://doi.org/10.1016/j.apcatb.2016.10.012.